Hybrid atom-molecule quantum walks in a one-dimensional optical lattice

Ling Lin (林凌),[1,2] Yongguan Ke (柯勇贯),[1,2] Chunshan He (何春山),[3,*] and Chaohong Lee (李朝红)[1,2,†]

[1]*Laboratory of Quantum Engineering and Quantum Metrology, School of Physics and Astronomy, Sun Yat-Sen University (Zhuhai Campus), Zhuhai 519082, China*

[2]*Key Laboratory of Optoelectronic Materials and Technologies, Sun Yat-Sen University (Guangzhou Campus), Guangzhou 510275, China*

[3]*School of Physics, Sun Yat-Sen University (Guangzhou Campus), Guangzhou 510275, China*

(Received 7 May 2018; revised manuscript received 8 August 2018; published 29 October 2018)

We study hybrid atom-molecule quantum walks in one-dimensional optical lattices with two interacting bosonic atoms which may be converted into a molecule. The hybrid atom-molecule energy bands include a continuum band and two isolated bands, which respectively correspond to scattering states and dressed bound states (DBSs). Because of the atom-molecule coupling, the DBSs may appear even in the absence of atom-atom interaction. From an initial state of two atoms occupying the same site, in addition to independent quantum walks which correspond to scattering states, correlated quantum walks appear as a signature of DBSs. Even if the atom-atom interaction and the atom-molecule coupling are much stronger than the tunneling strengths, independent quantum walks may still appear under certain resonant conditions. The correlated quantum walks show two light cones with different propagation velocities, which can be analytically explained by the effective tunneling strengths of the two different DBSs. Furthermore, the effective nearest-neighbor tunneling of DBSs can be suppressed to zero, which can be explained by the destructive interference between the atomic pair and the molecule.

DOI: 10.1103/PhysRevA.98.043628

I. INTRODUCTION

Quantum walks (QWs) [1], a direct result of quantum interference of different paths, have been extensively studied in both theory and experiments [2–5]. QWs can be exploited to various fields, from universal quantum computing [6], efficient quantum algorithm [7–11], and energy transfer [12] to topological state detection [13,14]. Single-particle QWs have already been implemented by various systems including ultracold atoms [15], ultracold ions [16], photonic waveguides [17], atomic spin impurities [18], etc. Moreover, it has also been demonstrated that single-particle QWs can be implemented via classical waves [19].

Beyond single-particle QWs, two-particle QWs have attracted extensive interest in recent years. The two-body physics in the standard Hubbard model has been studied thoroughly [20–23], where quasi-independent scattering states and repulsive or attractive bound states are found. The nonclassical correlation between noninteracting particles, i.e., the bunching and antibunching behavior, are found to depend strongly on the quantum statistical properties [24–26]. On the other hand, interaction between particles in a lattice is believed to be beneficial to universal quantum computation [27]. The interacting two-particle QWs have been broadly discussed and implemented in previous work [28–32]. The interaction is found to strongly affect the spatial correlations [33]. Particularly, the repulsively or attractively interacting (quasi)particles can form a bound pair [34,35] stabilized by the band gap. Therefore, besides the independent QWs, there is the cowalking of the bound pair [28,33,36].

Although the QWs of interacting particles have been extensively studied, it still remains unclear about the QWs involving atom-molecule coupling. According to the two-channel theory, a pair of atoms can be converted into a molecule and vice versa. For two bosons in optical lattices, due to the atom-molecule coupling, their energy spectrum includes two isolated bands and a continuum one [37–40]. The states in isolated bands are in superposition of atomic bound state and molecular state, which are called the dressed bound states (DBSs) in the following context. Under specific conditions, the DBSs can be tuned to enter the continuum band and thus lead to so-called scattering resonance [38]. For the Hubbard systems involving atom-molecule coupling, their two-body spectrum has been studied in Refs. [37–40] but the two-body quantum walks are not investigated. Since the QWs in these systems have not been revealed yet, it is worthy to investigate the dynamical properties of the hybrid atom-molecule systems. In particular, it is intriguing to explore the signature of DBSs via QWs.

In this article, by considering a one-dimensional (1D) Bose-Hubbard model with atom-molecule coupling, we study the QWs from two interacting Bose atoms occupying the same lattice site. Before investigating the hybrid atom-molecule QWs, we shall perform the calculation for the eigenenergies and the eigenstates to understand the property of the system. We focus on exploring the interplay among atom-molecule coupling, atom-atom interaction, and atom-molecule energy detuning and their effects on the QWs. Without the atom-atom interaction, there are two kinds of DBSs supported by pure atom-molecule coupling. Such an atom-molecule coupling

*stshcs@mail.sysu.edu.cn

†lichaoh2@mail.sysu.edu.cn; chleecn@gmail.com

may play the role of effective atom-atom interaction and then result in the correlated QWs. Due to the atom-molecule energy difference, the atom-atom interaction can be balanced under certain resonant conditions, which are derived explicitly. In this case, even if the background interaction is strong, the DBSs are broken into scattering states and there show the pattern of independent QWs.

By using the many-body degenerate perturbation theory, we give the effective models for the QWs of DBSs, in which the effective tunneling strengths of DBSs can be tuned by the atom-molecule energy difference. The effective model shows that the QWs of DBSs can be different. The dependence of effective tunneling DBSs on the molecular tunneling and atomic tunneling are of first and second order, respectively, indicating that even if the molecular tunneling is relatively weak, it may still have considerable effect on the DBS. Remarkably, from the effective model we find that the interplay between tunnelings of atoms and molecule can suppress the nearest-neighbor (NN) tunneling of DBSs.

The paper is organized as follows. In Sec. II, we introduce our hybrid atom-molecule system and solve its energy bands. In Sec. III, we present the QWs from two atoms occupying the same site. In particular, we discuss how the QWs are affected by the pure atom-molecule coupling (Sec. III A) and the interplay between atom-atom interaction and atom-molecule coupling (Sec. III B). In Sec. IV, we derive effective models for the QWs of DBSs and discuss the effective tunneling of DBSs. At last, we make a brief summary and discussion of our results.

II. HYBRID ATOM-MOLECULE ENERGY BANDS

We consider two interacting Bose atoms in 1D optical lattices, where the two atoms can be converted into a molecular state via atom-molecule coupling. The system obeys the Hamiltonian,

$$\begin{aligned}\hat{H} =& -\sum_{l=-L}^{L}\left(J_a\hat{a}_l^\dagger\hat{a}_{l+1}+J_m\hat{m}_l^\dagger\hat{m}_{l+1}+\text{H.c.}\right)\\&+\frac{U}{2}\sum_{l=-L}^{L}\hat{n}_l^a\left(\hat{n}_l^a-1\right)+g\sum_{l=-L}^{L}\left(\hat{a}_l^\dagger\hat{a}_l^\dagger\hat{m}_l+\text{H.c.}\right)\\&+\sum_{l=-L}^{L}\left(\varepsilon_a\hat{n}_l^a+\varepsilon_m\hat{n}_l^m\right).\end{aligned}\tag{1}$$

Here, g is on-site atom-molecule coupling strength, U is on-site background atom-atom interaction, $J_a(J_m)$ is the atomic(molecular) tunneling strength, $\varepsilon_a(\varepsilon_m)$ is the atomic(molecular) on-site energy, the lattice site index l ranges from $-L$ to L, the total number of lattice sites is $L_t = 2L+1$, and the periodic boundary condition (PBC) is imposed. The bosonic operators $\hat{a}_l^\dagger$ ($\hat{m}_l^\dagger$) and $\hat{a}_l$ ($\hat{m}_l$) create and annihilate an atom (molecule) on the lth site, respectively. Due to the fact that the mass of molecule composed by two atoms is two times larger than the single atom, the tunneling of the molecule is small compared with the tunneling of the atom [37–39,39,41,42]. Inclusion of relatively weak molecular tunneling is found to only slightly modify the spectrum [38]. Therefore, the tunneling of the molecule is usually omitted in previous work [39,41,42]. In this work, we shall keep all the terms of molecular tunneling in the analytical derivation, but only discuss it when it has non-negligible effect. The atom-molecule coupling g can be realized by applying the magnetoassociation [43] or photoassociation [44,45] technique. The on-site energy difference between atoms and molecule $\Delta = 2\varepsilon_m - \varepsilon_a$ can be tuned by applying external magnetic field [43].

Different from Refs. [37–40], we use an alternative method to obtain the eigenstates and eigenenergies of the system. The Hilbert space can be spanned by a complete set of orthogonal basis,

$$\mathcal{H}^{(2)} = \{|l_1l_2\rangle_a \oplus |j\rangle_m\}.\tag{2}$$

Here, $|j\rangle_m = \hat{m}_j^\dagger|\mathbf{0}\rangle(-L\leqslant j\leqslant L)$ denotes the state of one molecule in the jth lattice site, while $|l_1l_2\rangle_a = (1+\delta_{l_1l_2})^{-1/2}\hat{a}_{l_1}^\dagger\hat{a}_{l_2}^\dagger|\mathbf{0}\rangle$ $(-L\leqslant l_1\leqslant l_2\leqslant L)$ denotes the state of one atom in the l_1th site and one atom in the l_2th site, where $\delta_{l_1l_2}$ is the Kronecker delta function. Hence one can expand the eigenstates as $|\Phi\rangle = \sum_{l_1'\leqslant l_2'}\phi_{l_1'l_2'}|l_1'l_2'\rangle_a + \sum_{j'}\varphi_{j'}|j'\rangle_m$. Thus the eigenvalue problem $\hat{H}|\Phi\rangle = E|\Phi\rangle$ is described by the coupled equations:

$$\begin{aligned}&\sum_{l_1'\leqslant l_2'}\phi_{l_1'l_2'a}\langle l_1l_2|\hat{H}|l_1'l_2'\rangle_a+\sum_{j'}\varphi_{ja}\langle l_1l_2|\hat{H}|j'\rangle_m=E\phi_{l_1l_2},\\&\sum_{j'}\varphi_{j'm}\langle j|\hat{H}|j'\rangle_m+\sum_{l_1'\leqslant l_2'}\phi_{l_1l_2m}\langle j|\hat{H}|l_1'l_2'\rangle_a=E\varphi_j.\end{aligned}\tag{3}$$

For simplicity, we define $\psi_{l_1'l_2'} = (1+\delta_{l_1'l_2'})^{1/2}\phi_{l_1'l_2'}$ so that the normalization coefficient is eliminated. After some algebraic calculation, using commutation relations of bosonic operators, one can obtain

$$\begin{aligned}E\psi_{l_1,l_2} =& -J_a\left(\psi_{l_1,l_2+1}+\psi_{l_1+1,l_2}+\psi_{l_1-1,l_2}+\psi_{l_1,l_2-1}\right)\\&+\delta_{l_1,l_2}U\psi_{l_1,l_2}+2\varepsilon_a\psi_{l_1,l_2}+2g\delta_{l_1,j}\delta_{l_2,j}\varphi_j,\end{aligned}\tag{4a}$$

$$E\varphi_j = -J_m(\varphi_{j+1}+\varphi_{j-1})+\varepsilon_m\varphi_j+g\delta_{l_1j}\delta_{l_2j}\psi_{l_1,l_2}.\tag{4b}$$

Obviously, Eq. (4a) and Eq. (4b) show the hybridization of atomic and molecular states. To solve these equations, we adopt the ansatz

$$\psi_{l_1,l_2} = C_ae^{iK_aR_a}\xi(r),\quad \varphi_j = C_me^{iK_mR_m}.\tag{5}$$

Here, K_a, $R_a = (l_1+l_2)/2$ and $r = l_2 - l_1$ are respectively the center-of-mass (c.m.) quasimomentum, c.m. position, and relative position of atoms. Correspondingly, K_m and $R_m = j$ are the molecular quasimomentum and position, respectively. The coefficients C_a and C_m are the normalization constants. The function $\xi(r)$ is independent of K_a and R_a,

$$\xi(r) = C_+e^{ik|r|}+C_-e^{-ik|r|},\tag{6}$$

where k can be real or complex and $C_\pm$ are unknown coefficients. From the physical point of view, the states of atoms ψ_{l_1,l_2} can be expressed as Bloch-like functions with independent c.m. part and relative motion part.

Before we go further, let us prove that $K_a = K_m = K$ for eigenstates. When $l_1 = l_2 = j$ $(R_m = R_a = R)$, combining

Eq. (4b) and Eqs. (5), we have

$$\frac{E+2J_m\cos(K_m)-\epsilon_m}{g}C_m e^{i(K_m-K_a)R}=\xi(0)C_a. \quad (7)$$

Because Eq. (7) holds for all $R\in[-L,L]$, we have $K_m=K_a$. For simplicity, we denote $K_m=K_a=K$ and restrict it in the first Brillouin zone from now on. Since the PBC requires $\psi_{l_1,l_2+L_t}=\psi_{l_1+L_t,l_2}=\psi_{l_1,l_2}$ and $\varphi_{j+L_t}=\varphi_j$, the c.m. quasimomentum obeys $K=2\pi n/L_t$ with $n=-L,-L+1,\ldots,L$.

From Eqs. (4) and (5), denoting $\tilde{E}=E-2\varepsilon_a$ and $\Delta=\varepsilon_m-2\varepsilon_a$, one can obtain

$$\tilde{E}\xi(r)=J_a^K[\xi(r+1)+\xi(r-1)]+\delta_{r,0}U_{\rm eff}\xi(r), \quad (8)$$

where $U_{\rm eff}=U+2g^2/(\tilde{E}-\Delta-J_m^K)$ and $J_a^K=-2J_a\cos(K/2)$, $J_m^K=-2J_m\cos(K)$. Obviously, the atom-molecule coupling contributes an additional energy-dependent term in the effective interaction $U_{\rm eff}$. This indicates that the atom-molecule coupling g may play the role of atom-atom interaction U and therefore DBSs may appear even when the atom-atom interaction is absent.

In the case of $\Delta\to\infty$ or $U\to\infty$, Eq. (8) can be approximated as

$$\tilde{E}\xi(r)=J_a^K[\xi(r+1)+\xi(r-1)]+\delta_{r,0}U\xi(r), \quad (9)$$

which reduces to the case of no atom-molecule coupling [21].

A. Continuum band

The continuum band corresponds to scattering states whose k are real numbers. For a real k, substituting Eq. (6) into Eq. (8), we have the eigenenergies

$$\tilde{E}=2J_a^K\cos(k). \quad (10)$$

Here, the value of k can be determined by the following procedure. Substituting Eqs. (6) and (10) into Eq. (8), one can find that the coefficients $C_\pm$ obey

$$\frac{C_+}{C_-}=-\frac{-J_a^K 2i\,\sin k+\left(U+\frac{2g^2}{2J_K\cos k-\Delta-J_m^K}\right)}{J_a^K 2i\,\sin k+\left(U+\frac{2g^2}{2J_K\cos k-\Delta-J_m^K}\right)}. \quad (11)$$

Furthermore, according to the PBC, $\xi(r)$ obeys $\xi(r+L_t)=e^{iKL_t/2}\xi(r)$ and therefore one can obtain the coefficients $C_\pm$

$$\frac{C_+}{C_-}=-\frac{(-1)^{iKL_t/2}-e^{-ikL_t}}{(-1)^{iKL_t/2}-e^{ikL_t}}. \quad (12)$$

Combining Eqs. (11) and (12), one can determine k by solving the following equation:

$$\frac{J_a^K 2i\,\sin k-\left(U+\frac{2g^2}{2J_K\cos k-\Delta-J_m^K}\right)}{J_a^K 2i\,\sin k+\left(U+\frac{2g^2}{2J_K\cos k-\Delta-J_m^K}\right)}=(-1)^{KL_t/2}e^{-ikL_t}. \quad (13)$$

Obviously, the above equation is invariant under the transformation $k\to-k$ and thus k can be restrained in the region $[0,\pi]$. Substituting the values of k into Eq. (10), we obtain the eigenenergies of scattering states, which are denoted by the circular dots in Fig. 1. Correspondingly, the explicit expression of $\xi(r)$ is given as

$$\xi(r)\sim(-1)^{KL_t/2}e^{-ikL_t}e^{ik|r|}+e^{-ik|r|}, \quad (14)$$

which has the same form as the one of no atom-molecule coupling [21,33].

Besides, we calculate the proportion of molecular state for each eigenstate,

$$P_m=\sum_j|\varphi_j|^2, \quad (15)$$

which is denoted by the color in Fig. 1. Due to the atom-molecule coupling, the scattering states are a hybridization of molecular states and atomic states.

B. Isolated bands

Isolated bands correspond to the states with complex values of k. If the atom-molecule coupling is absent, i.e., $g=0$, the atomic and molecular states are decoupled and there appears an isolated band corresponding to the molecular states; see Fig. 1(a1). When $J_m=0$, the isolated molecular band is exactly given as $\tilde{E}=\Delta$.

For nonzero atom-molecule couplings g, the isolated bands correspond to DBSs, whose k can be assumed as $k=\beta+i\eta$ (where β and η are both real numbers). Noting that the wave function must remain finite when $r\to\infty$, Eq. (6) can be rewritten as

$$\xi(r)=e^{(i\beta-\eta)|r|}. \quad (16)$$

For simplicity, we introduce $e^{i\beta-\eta}\equiv\alpha$, which satisfies $\alpha\in\mathbb{C}$ and $0<|\alpha|<1$. Thus $\xi(r)$ can be rewritten as

$$\xi(r)=\alpha^{|r|}. \quad (17)$$

This expression indicates that the wave functions of atomic states decay exponentially when the relative distance increases [21]. Combining Eqs. (8) and (17), one can obtain

$$\tilde{E}=2J_a^K\alpha+\left(U+\frac{2g^2}{\tilde{E}-\Delta-J_m^K}\right) \quad (18)$$

for $r=0$ and

$$\tilde{E}=J_a^K(\alpha^{-1}+\alpha) \quad (19)$$

for $r>0$. Here, $\tilde{E}$ and α are unknown parameters. To ensure real eigenenergies $\tilde{E}$, the parameter α must be real as well so that we have $\beta=m\pi$ and $m\in\mathbb{N}$. By numerically solving Eqs. (18) and (19), we obtain two isolated bands for DBSs; see the triangular dots in Fig. 1. The emergence of two isolated bands is consistent with the previous results obtained by other methods [37–39]. From Eqs. (18) and (19), when $J_m=U=\Delta=0$, we find that if $(\tilde{E},\alpha)$ are their solutions, then $(-\tilde{E},-\alpha)$ are also their solutions. Furthermore, when the atom-molecule coupling strength g increases, the two symmetric and isolated bands gradually separate from the continuum band; see Figs. 1(a1)–1(a4), respectively.

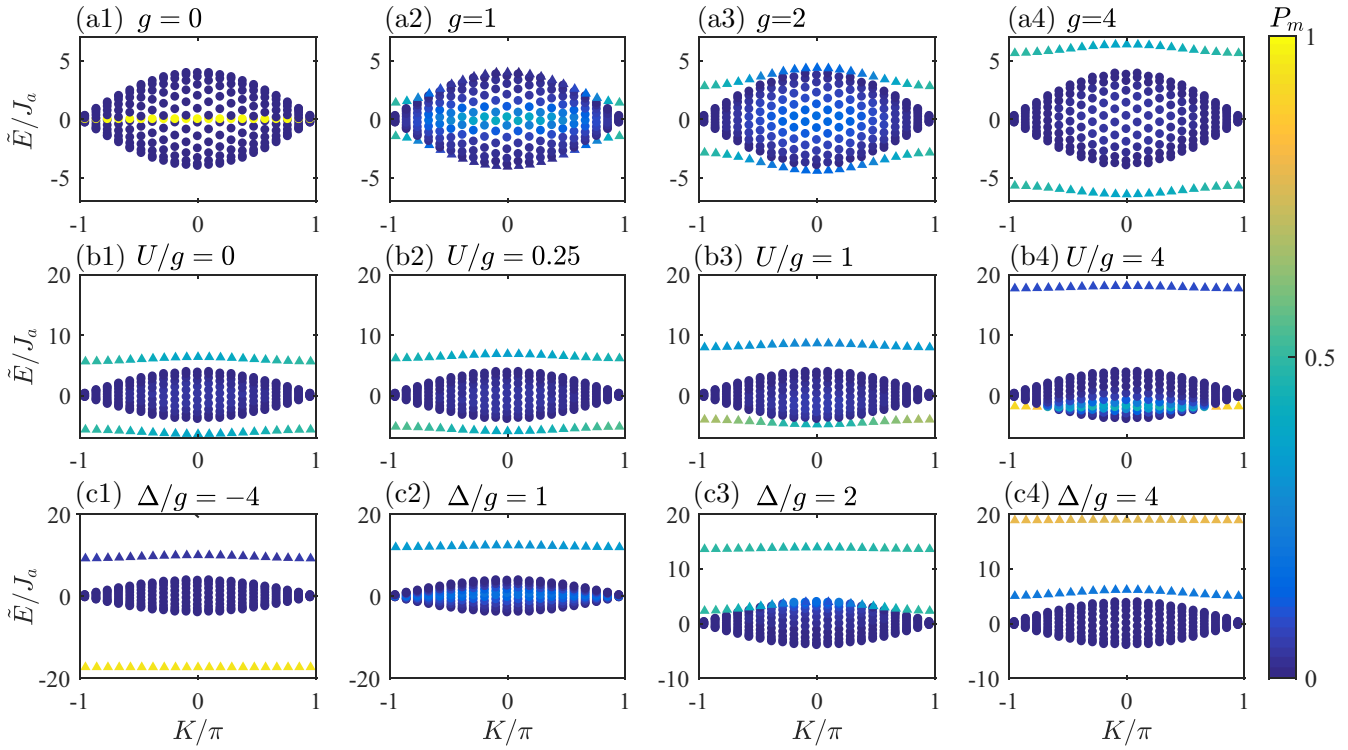

FIG. 1. Energy spectrum under influence of atom-molecule coupling, atom-atom interaction, and atom-molecule energy difference. The circular and triangular dots denote the scattering states and the DBSs, respectively. The color of each dot represents the proportion of molecular states, which is given by $P_m = \sum_j |\varphi_j|^2$. (a1)–(a4) Energy spectrum for different atom-molecule coupling $g = 0, 1, 2, 4$ with $U = \Delta = 0$. (b1)–(b4) Energy spectrum for different atom-atom interaction $U/g = 0, 0.25, 1, 4$ with $\Delta = 0$ and $g = 4$. (c1)–(c4) Energy spectrum for atom-molecule energy difference $\Delta/g = -4, 1, 2, 4$ with $g = 4$, $U = 8$. The other parameters are set as $J_a = 1$, $J_m = 0$, and $L_t = 21$ by default. Since the molecular tunneling strength J_m is much smaller than the atomic tunneling strength J_a in reality, we omit it in the numerical calculation if it only brings small modification to the spectrum for simplicity.

C. Interplay among the atom-molecule coupling, the atom-atom interaction, and the atom-molecule energy difference

Below, given $g = 4J_a = 4$ and $J_m = 0$, we will show how the atom-atom interaction (U) and the atom-molecule energy difference (Δ) affect the energy spectrum.

To explore the interplay of g and U, we choose $\Delta = 0$. For simplicity, we concentrate our discussion on the case of $U > 0$. Actually, the following discussion can be easily applied to the case of $U < 0$. We present the energy bands for different values of U/g in Figs. 1(b1)–1(b4). Clearly, the repulsive interaction gradually lifts the energy of isolated bands. Under strongly repulsive interaction, the lower isolated band enters into the continuum band and results in the resonance between scattering and bound states [37,38]; see Fig. 1(b4). Around resonance, the states display stronger hybridization than other states in the continuum band. When U approaches infinity, from Eq. (8), the eigenenergies for the lower and upper isolated bands are given as $\tilde{E} = \Delta$ and $\tilde{E} = U$, respectively. In this instance, the lower isolated band purely corresponds to the bare molecule, while the upper isolated band corresponds to the bounded atomic pair.

Given finite atom-atom interaction $U/g = 2$, we then explore the interplay between Δ and g, as shown in Figs. 1(c1)–1(c4). When $\Delta/g \ll -1$, the upper and lower isolated bands are respectively dominated by the bounded atomic pairs and the molecular states; see Fig. 1(c1). With the increase of Δ, the lower isolated band is gradually shifted from the bottom to the upper of the continuum band; see Figs. 1(c2) and 1(c3). Particularly, for certain values of Δ, the lower isolated band may completely merge into the continuum band, as shown in Fig. 1(c2). When $\Delta/g \gg 1$, the lower isolated band becomes dominated by the bounded atomic pair and the upper isolated band tends to be dominated by the molecular states; see Fig. 1(c4).

However, if the atom-atom interaction is zero, the lower isolated band will never merge into the continuum band. To show this, we plot the eigenenergies for given c.m. quasimomentum $K = 0$ as a function Δ; see Fig. 2. In the absence of atom-atom interaction ($U = 0$), the lower (upper) isolated band gradually approaches the bottom (above) boundary of the continuum band when $\Delta \to +\infty$ ($\Delta \to -\infty$); see Fig. 2(a). The two isolated bands for DBSs always sandwich the continuum band. For nonzero atom-atom interaction ($U \neq 0$), the energy of DBSs can merge into the continuum band, causing the resonance between DBSs and continuum band; see Fig. 2(b). In fact, one can prove that, for a given K, there are two DBS solutions if $U = 0$ and $g \neq 0$, while there can be only one solution if $U \neq 0$; see Appendix A for more details. To summarize, the atom-atom interaction is essential for the occurrence of the resonance.

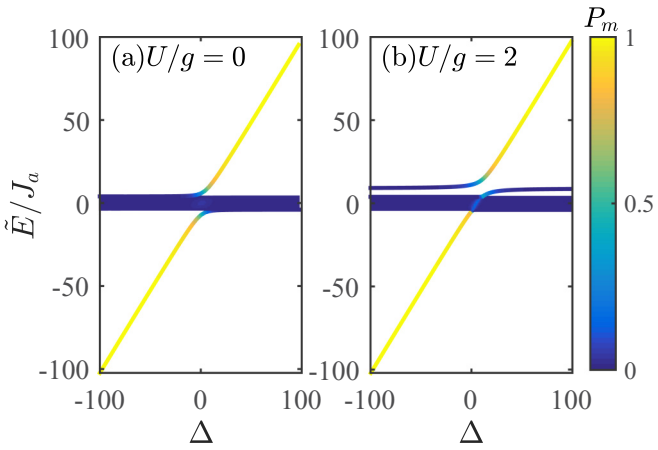

FIG. 2. Eigenenergies of the zero quasimomentum states ($K = 0$) versus the energy difference Δ and different ratios: (a) $U/g = 0$ and (b) $U/g = 2$. The color represents the proportion of molecular states, which is given by $P_m = \sum_j |\varphi_j|^2$. The other parameters are chosen as $J_a = 1$, $J_m = 0$, $g = 4$, and $L_t = 21$.

D. Resonance between scattering states and DBSs

In this subsection, we discuss the resonance between scattering states and DBSs, which is usually characterized as the Fano-Feshbach resonance [37,38], and give the resonant conditions.

From Eqs. (18) and (19), one can solve the energies for two isolated bands of DBSs. However, as mentioned in the previous subsection, for nonzero atom-atom interaction U we have proved that there may be only one solution under some specific conditions. For a given K, the condition of only one solution of DBSs is given as

$$\frac{2g^2}{U} - 2\left|J_a^K\right| - J_m^K < \Delta < \frac{2g^2}{U} + 2\left|J_a^K\right| - J_m^K. \tag{20}$$

This indicates that there exists resonance between scattering states and DBSs. If $J_m = 0$, from Eq. (20), one can find that there is only one DBS solution for all K when $\Delta = 2g^2/U$, exactly corresponding to the result mentioned above in Fig. 1(c2).

The resonance can be understood by the atom-molecule conversion in the limit of $J_a = J_m = 0$; see Appendix. B. By solving the eigenequation, one can obtain three different kinds of eigenstates. One kind of eigenstate corresponds to separated atomic states $|a_{l_1 l_2}\rangle = |l_1 l_2\rangle_a$ with $l_1 < l_2$. The other two kinds of eigenstates correspond to the *dressed-molecule states*, which are in superposition of the atomic state and molecular state $|d_l\rangle = A_\sigma |l\rangle_m + B_\sigma |l, l\rangle_a$. Here A_σ and B_σ are the coefficients of lower ($\sigma = 1$) and upper ($\sigma = 2$) dressed-molecule states. The lower dressed-molecule states and the separated atomic states are degenerate when $\Delta = 2g^2/U$ ($U > 0$). Under this condition, a tiny atomic tunneling will immediately make the separated atomic states into the atomic scattering states, and then the atomic scattering states couple with the dressed-molecule states. That is why the degenerate condition is identical to the condition where the lower isolated band merges into the continuum band.

In addition, due to the interplay between different interactions, the scattering resonance has also been found [46,47]. For an example, due to the interplay between the on-site and nearest-neighbor interactions [46], the bound states may merge into the continuum band. Similarly, in our hybrid atom-molecule system, the interplay between atom-molecular coupling (which results in an effective atom-atom interaction) and the background atom-atom interaction may induce the scattering resonance.

III. HYBRID ATOM-MOLECULE QUANTUM WALKS

In this section, we analyze the QWs in our atom-molecule Hubbard system (1). The initial state is chosen as $|\Psi(0)\rangle = |0, 0\rangle_a$, in which both atoms occupy the zeroth lattice site. The time evolution is governed by the Schrödinger equation,

$$|\Psi(t)\rangle = e^{-i\hat{H}t}|\Psi(0)\rangle. \tag{21}$$

The atomic and molecular density distributions are respectively defined as

$$\begin{aligned} n_{a,l}(t) &= \langle\Psi(t)|a_l^\dagger a_l|\Psi(t)\rangle, \\ n_{m,l}(t) &= \langle\Psi(t)|m_l^\dagger m_l|\Psi(t)\rangle. \end{aligned} \tag{22}$$

The spatial correlation of atoms is characterized by a second-order correlation function,

$$\Gamma_{l_1 l_2}(t) = \langle\Psi(t)|a_{l_1}^\dagger a_{l_2}^\dagger a_{l_2} a_{l_1}|\Psi(t)\rangle, \tag{23}$$

which relates to the probability $P_{l_1,l_2}(t) = |\langle l_1, l_2|\Psi(t)\rangle|^2$ via $\Gamma_{l_1 l_2}(t) = (1 + \delta_{l_1,l_2})P_{l_1,l_2}(t)$. Thus $\Gamma_{l_1 l_2}(t)$ gives the probability of detecting one particle at l_1th site and the other particle at l_2th site in the meantime. The diagonal terms $\Gamma_{l_1=l_2}(t)$ describe the correlated QWs of two atoms, in which the two atoms walk as a whole. The nondiagonal terms $\Gamma_{l_1\neq l_2}(t)$ describes the independent QWs of two atoms.

If there is no atom-molecule coupling, the time evolution from the initial state $|0, 0\rangle_a$ will evolve only in the subspace of the atomic states. Since the molecular subspace is not involved, the QWs of atoms are expected to only depend on J_a/U. When the atom-atom interaction is weak, the initial state has large overlaps with the atomic scattering states so that the time evolution is dominated by independent QWs [33]. When the atom-atom interaction is strong, the two atoms in the same site will form a stable bound state so that the time evolution is dominated by correlated QWs [21,33,35,39].

Indeed, under strong interaction, two atoms do perform correlated QWs, that is, the correlation function is dominated by the diagonal terms which recovers the results in Ref. [33].

A. QWs with atom-molecule coupling

Since the atom-molecule coupling may play the role of effective interaction, to show how the atom-molecule coupling affects the QWs, we turn off the atom-atom interaction ($U = 0$) and the atom-molecule energy difference ($\Delta = 0$).

For comparison, we simulate the QWs with $g = 0$ and $g = 10$. The tunneling of atoms and molecule are chosen as $J_a = 1$, $J_m = 0$. Without atom-molecule coupling, the time evolution of atomic density distribution and the final correlation function are shown in Figs. 3(a) and 3(b). The correlation function is dominated by the off-diagonal terms, which indicates that the two atoms walk independently.

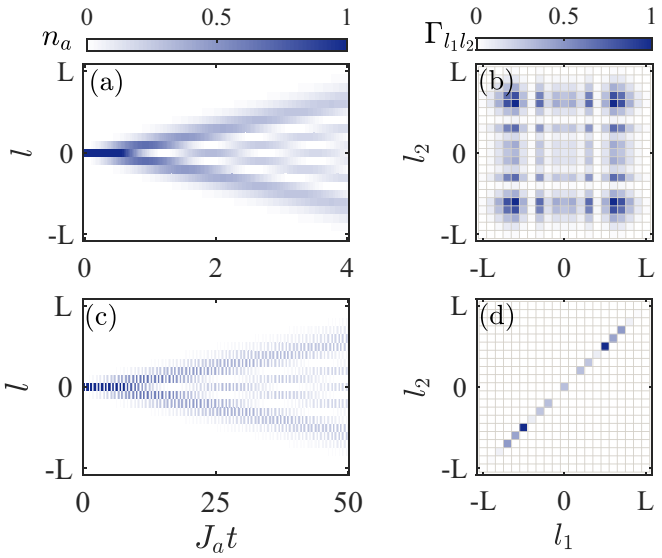

FIG. 3. QWs with (a),(b) zero atom-molecule coupling $g/J_a = 0$ and (c),(d) strong atom-molecule coupling $g/J_a = 10$. The left column shows the time evolution of atomic density distribution and the right column shows correlation functions of atoms for the final state. The other parameters are chosen as $J_a = 1$, $J_m = 0$, $U = 0$, $\Delta = 0$, and $L_t = 21$.

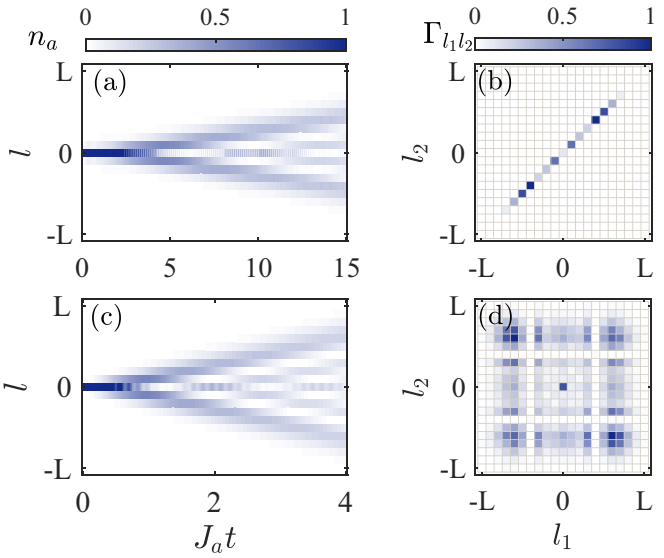

FIG. 4. Hybrid atom-molecule QWs under (a),(b) nonresonant condition $\Delta = -40 \ll 2g^2/U$ and (c),(d) resonant condition $\Delta = 40 = 2g^2/U$. The left column shows the time evolution of atomic density distribution and the right column shows correlation functions of atoms for the final state. The other parameters are chosen as $J_a = 1$, $J_m = 0$, $U = 5$, $g = 10$, and $L_t = 21$.

At the presence of atom-molecule coupling, there will be the atom-molecule Rabi oscillations [48,49]. If the atom-molecule coupling is strong enough, the atoms would go through many times of conversion before they walk to nearby lattice sites and thus experience a larger effective interaction. In Figs. 3(c) and 3(d), we show the atomic density distribution and the final correlation function for $g = 10$ and $\Delta = 0$. There appears notable stripes in the time propagation of atomic density distribution, which can be explained by the fast atom-molecule conversion induced by strong atom-molecule coupling; see Fig. 3(c). The strongly correlated QWs are also identified by the final correlation functions which are dominated by diagonal terms; see Fig. 3(d). This is because the effective interaction is much larger than the tunneling strength, $U_{\text{eff}} = 2g^2/(\tilde{E} - \Delta - J_m^K) \gg J_a$.

However, even for strong atom-molecule coupling, correlated QWs disappear when the atom-molecule energy difference Δ is much larger than the atom-molecule coupling g. In such a situation, the larger atom-molecule energy difference makes the atom-molecule conversion negligible. Therefore, atomic and molecular states are nearly decoupled and the two atoms walk independently since there is negligible effective atom-atom interaction from the atom-molecule conversion.

B. QWs near the resonance between scattering states and DBSs

In the above, we show that the time evolution is either dominated by independent QWs or correlated ones. We wonder whether independent and correlated QWs may coexist. As mentioned in Sec. II D, under the conditions of $g \gg J_{a,m}$ and $U \gg J_{a,m}$, the resonance between scattering states and DBSs takes place around $\Delta \simeq 2g^2/U$. Below we will show the coexistence of independent and correlated QWs near the resonance between scattering states and DBSs.

Given $J_a = 1$, $J_m = 0$, $g = 10$, and $U = 5$, we present the QWs in nonresonant ($\Delta = -40 \ll 2g^2/U$) and resonant ($\Delta = 40 = 2g^2/U$) conditions; see Fig. 4. Compared with Fig. 3(c), there are no clear stripes in the time propagation of atomic density distribution for large Δ; see Figs. 4(a) and 4(c). This is because large atom-molecule energy difference suppresses the atom-molecule conversion. In the nonresonant condition, the diagonal elements of correlation function dominate after the time evolution, indicating the strong cowalking behavior; see Fig. 4(b). In the resonant condition, however, in addition to significant off-diagonal elements near the boundaries, there are significant diagonal elements on the diagonal line in the final correlation function; see Fig. 4(d). This indicates the coexistence of independent and correlated QWs, although the propagation speed of correlated QWs is smaller than the one of independent QWs. Such a process can be explained by our argument in Sec. II D.

IV. EFFECTIVE SINGLE-PARTICLE MODEL FOR STRONGLY CORRELATED QUANTUM WALKS

The strongly correlated QWs can be described by a single-particle model. By employing the many-body quantum degenerate perturbation theory [50], we derive an effective single-particle Hamiltonian for the strongly correlated QWs.

To avoid the breakdown of DBSs near the resonance between scattering states and DBSs, we suppose $|\Delta - 2g^2/U| \gg 0$. When $J_{a,m} \ll g$ or $J_{a,m} \ll U$, the tunneling term $\hat{T} = -\sum (J_a \hat{a}_l^\dagger \hat{a}_{l+1} + J_m \hat{m}_l^\dagger \hat{m}_{l+1} + \text{H.c.})$ in Hamiltonian (1) can be treated as a perturbation. Defining the subspace $\mathcal{H}_\sigma^d = \{|d_{\sigma,l}\rangle, -L \leqslant l \leqslant L\}$ for DBSs (see Appendix B), the projection operator is given by projecting the full Hilbert

space $\mathcal{H}^{(2)}$ onto the unperturbed subspace $\mathcal{H}_\sigma^d$,

$$\hat{P}_\sigma = \sum_l |d_{\sigma,l}\rangle\langle d_{\sigma,l}|, \tag{24}$$

where $\sigma = \{1, 2\}$ denotes the index for two different kinds of DBSs. Besides, the projection onto the orthogonal complement of $\mathcal{H}_\sigma^d$ reads as

$$\begin{aligned}\hat{S}_\sigma = &\sum_{E_{l_1 l_2}^{(0)} \neq E_\sigma^{(0)}} \frac{1}{E_\sigma^{(0)} - E_{l_1 l_2}^{(0)}} |l_1 l_2\rangle\langle l_1 l_2| \\ &+ \sum_{l,\sigma' \neq \sigma} \frac{1}{E_\sigma^{(0)} - E_{\sigma'}^{(0)}} |d_{\sigma',l}\rangle\langle d_{\sigma',l}|. \end{aligned} \tag{25}$$

Therefore, according to the perturbation theory [50] up to second order, we have

$$\begin{aligned}\hat{H}_\sigma^{\text{eff}} &= \hat{h}_{\sigma,0} + \hat{h}_{\sigma,1} + \hat{h}_{\sigma,2} \\ &= E_\sigma \hat{P}_\sigma + \hat{P}_\sigma \hat{T} \hat{P}_\sigma + \hat{P}_\sigma \hat{T} \hat{S}_\sigma \hat{T} \hat{P}_\sigma. \end{aligned} \tag{26}$$

Substituting the projection operators and perturbation term into the above equation, we can obtain

$$\hat{h}_{\sigma,0} = E_\sigma \sum_l |d_{\sigma,l}\rangle\langle d_{\sigma,l}|, \tag{27}$$

$$\hat{h}_{\sigma,1} = -J_m A_\sigma^2 \sum_l (|d_{\sigma,l}\rangle\langle d_{\sigma,l+1}| + |d_{\sigma,l+1}\rangle\langle d_{\sigma,l}|), \tag{28}$$

$$\begin{aligned}\hat{h}_{\sigma,2} = &\frac{2{J_a}^2 B_\sigma^2}{E_\sigma^{(0)} - E_{l_1,l_2}^{(0)}} \sum_l \begin{pmatrix} 2|d_{\sigma,l}\rangle\langle d_{\sigma,l}| \\ +|d_{\sigma,l+1}\rangle\langle d_{\sigma,l}| + \text{H.c.} \end{pmatrix} \\ &+ \frac{{J_m}^2 A_1^2 A_2^2}{E_\sigma^{(0)} - E_{\sigma'}^{(0)}} \sum_l \begin{pmatrix} 2|d_{\sigma,l}\rangle\langle d_{\sigma,l}| \\ +|d_{\sigma,l+2}\rangle\langle d_{\sigma,l}| + \text{H.c.} \end{pmatrix}. \end{aligned} \tag{29}$$

Here, the coefficients A_σ and B_σ are given by calculating the unperturbed time-independent Schrödinger equation (see Appendix B).

By introducing the mapping, $|d_l\rangle\langle d_l| \Leftrightarrow {d_l}^\dagger d_l$, $|d_l\rangle\langle d_{l+1}| \Leftrightarrow {d_l}^\dagger d_{l+1}$, $|d_{l+1}\rangle\langle d_l| \Leftrightarrow {d_{l+1}}^\dagger d_l$, the effective single-particle Hamiltonian can be written as

$$\begin{aligned}\hat{H}_\sigma^{\text{eff}} = &\sum_l \left(E_\sigma^{(0)} + \frac{4{J_a}^2 B_{1,2}^2}{E_\sigma^{(0)} - E_{l_1,l_2}^{(0)}} + 2\frac{{J_m}^2 A_1^2 A_2^2}{E_\sigma^{(0)} - E_{\sigma'}^{(0)}} \right) {d_{\sigma,l}}^\dagger d_{\sigma,l} \\ &+ \left(\frac{2{J_a}^2 B_\sigma^2}{E_\sigma^{(0)} - E_{l_1,l_2}^{(0)}} - J_m A_\sigma^2 \right) \sum_j ({d_{\sigma,l}}^\dagger d_{\sigma,l+1} + \text{H.c.}) \\ &+ \left(\frac{{J_m}^2 A_1^2 A_2^2}{E_\sigma^{(0)} - E_{\sigma'}^{(0)}} \right) \sum_l ({d_{\sigma,l}}^\dagger d_{\sigma,l+2} + \text{H.c.}). \end{aligned} \tag{30}$$

In addition to the nearest-neighbor (NN) tunneling, there appears the next-nearest-neighbor (NNN) tunneling, which originates from the effects of molecular tunneling. The NNN tunneling brought by the atomic tunneling can be derived from third-order perturbation theory, and we have neglected it since this term is extremely small compared with the lower order terms. Since $|E_1^{(0)} - E_2^{(0)}| \gg |E_1^{(0)} - E_0^{(0)}|$ or $|E_2^{(0)} - E_0^{(0)}|$, the NNN tunneling term is generally negligible compared with other terms. By implementing a Fourier transformation,

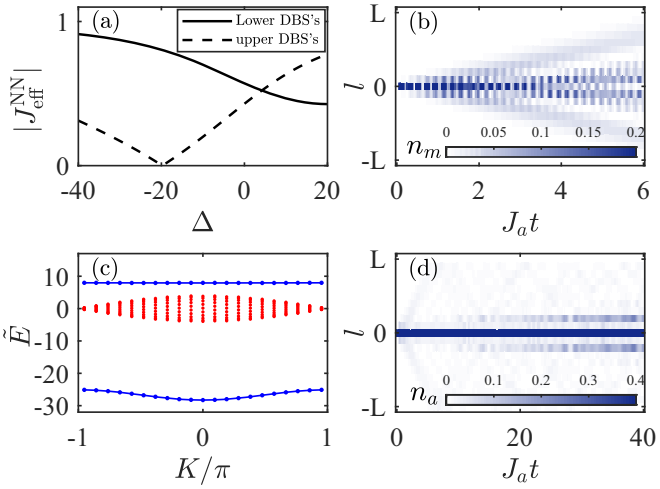

FIG. 5. (a) Effective nearest-neighbor tunneling strength J_{eff}^{NN} versus the atom-molecule energy difference Δ. The parameters are chosen as $J_a = J_m = 1$, $g = 10$, and $U = 0$. (b) Time evolution of molecular density distribution with $\Delta = -10$ and the same parameters with (a). (c) The energy bands with $\Delta = -19.125$, $L_t = 21$, and other parameters given in (a). The blue-dotted lines and the red dots correspond to the bands of DBSs and atomic scattering states, respectively. (d) Long time evolution of atomic density distribution with $\Delta = -19.125$ and other parameters given in (a).

the above single-particle Hamiltonian can be easily diagonalized and the eigenenergies are given as

$$\begin{aligned}E_\sigma^{\text{eff}} = &\left(\frac{8{J_a}^2 B_\sigma^2}{E_\sigma^{(0)} - E_{l_1,l_2}^{(0)}} - 4J_m A_\sigma^2 \right) \cos^2\left(\frac{K}{2}\right) \\ &+ 4\frac{{J_m}^2 A_1^2 A_2^2}{E_\sigma^{(0)} - E_{\sigma'}^{(0)}} \cos^2 K + E_\sigma^{(0)} + 2J_m A_\sigma^2, \end{aligned} \tag{31}$$

which are well consistent with the ones from numerical diagonalization of the original Hamiltonian.

In the effective single-particle Hamiltonian (30), the effective NN tunneling strength is given as $J_{\text{eff},\sigma}^{NN} = 2{J_a}^2 B_\sigma^2/(E_\sigma^{(0)} - E_{l_1,l_2}^{(0)}) - J_m A_\sigma^2$. Obviously, $J_{\text{eff},\sigma}^{NN}$ also depends on the atom-molecule energy difference Δ. In Fig. 5(a), we plot $J_{\text{eff},\sigma}^{NN}$ as a function of Δ, in which the solid and dashed lines respectively correspond to the upper and lower DBS bands. The parameters are chosen as $J_a = J_m = 1$, $g = 10$, and $U = 0$. The effective tunneling strengths for the upper and lower DBS bands are always different except for the crossing point. The different effective tunneling strength will result in different propagation speeds in QWs. In Fig. 5(b), we show the atomic density distribution with $\Delta = -10$ and other parameters the same as the ones for Fig. 5(a). Since the initial state mostly occupies the two DBS bands, there appear two light cones: the inner light cone and the outer one respectively correspond to the QWs of DBSs in the upper and lower bands.

From Fig. 5(a), near $\Delta = -19.125$, the effective tunneling strength of the DBSs in the upper band is almost zero, i.e., $J_{\text{eff}}^{NN} \approx 0$. Given $\Delta = -19.125$, we plot the energy bands in Fig. 5(c). The upper DBS band is very flat, which indicates very small tunneling strength, while the lower DBS band is not. This is concordant with the results of the effective

model in Fig. 5(a). Noticing that $J_{\text{eff}}^{NN} \approx 0$, there is only the NNN tunneling term ($J_{\text{eff}}^{NNN} \simeq 0.005$) in the effective Hamiltonian (30). Therefore, the odd sites are never occupied in the QWs from the zeroth site, which is clearly significant of the NNN tunneling; see Fig. 5(d). Such a phenomenon can be understood as the coherent interference between the atomic and molecular tunneling. As shown in the perturbative calculation, the effective NN tunneling of DBSs can be achieved via two paths, one of which is the second-order atomic tunneling and the other one the first-order molecular tunneling. These two paths give rise to different values of effective tunneling energy. When these two values have opposite values with the same magnitude, the total effective tunneling is canceled out.

On the other hand, in the effective Hamiltonian (30), the effective tunneling induced by the molecular tunneling is of first order, while the effective tunneling induced by atomic tunneling is of second order. This means that, as the molecular tunneling may have considerable effects, it should be treated carefully in realistic systems.

V. SUMMARY AND DISCUSSIONS

In summary, we study the energy bands and hybrid atom-molecule QWs of a 1D coupled atom-molecule Hubbard system. We find that the atom-molecule coupling can play the role of effective atom-atom interaction. Unlike the conventional bounded atomic pair, the cooperation of the atom-atom interaction and the atom-molecule coupling induces two kinds of DBSs, which are the dressed molecule states in superposition of bounded atomic pair and bare molecule. Even if the atom-atom interaction is absent, one can observe correlated QWs induced by the atom-molecule coupling. Tuning the parameters (the atom-molecule energy difference Δ, the atom-atom interaction U, and the atom-molecule coupling g) to satisfy the resonant condition, one of the DBSs will enter the continuum band and break into atomic scattering states. Thus one can observe the coexistence of independent and correlated QWs near the resonance between scattering states and DBSs. Away from the resonant condition, we employ many-body quantum degenerate perturbation theory to derive the effective single-particle Hamiltonian for the two DBS bands. The nearest-neighbor tunneling strength in the effective single-particle model can be turned off by tuning the atom-molecule energy difference Δ. Due to the two DBSs having different effective tunneling strengths, the QWs show two light cones with different propagation speeds. Moreover, we find that the NN tunneling of one of the DBSs can be suppressed to zero due to the interference between atomic tunneling and molecular tunneling. In this condition, the NNN tunneling becomes dominated and can be observed from the distribution of atomic density during the time evolution.

Our study not only provides a full description for the hybrid atom-molecule QWs with atom-molecule coupling, but also will shine some light on the two-photon QWs with spontaneous parametric down-conversion (SPDC) [51–53]. In such a waveguide array, the near-degenerate signal and idler photons correspond to two identical atoms, the pump photon acts as the molecule, and the SPDC plays the role of the atom-molecule coupling. The difference is that, in the waveguide array, the energy of signal and idler photons always equal the pump photon, and there is no interaction between photons if the Kerr effects are absent. According to our study, the idler and signal photons may have effective on-site interaction induced by the SPDC even if there are no Kerr effects [54]. Furthermore, the idler and signal photons can form dressed bound states with the pump photon when the SPDC is sufficiently strong. Therefore, there will appear two different kinds of dressed photonic bound states with different effective hopping strengths between waveguides.

ACKNOWLEDGMENT

This work is supported by the National Natural Science Foundation of China (NNSFC) under Grants No. 11874434 and No. 11574405.

APPENDIX A: GRAPHICAL ILLUSTRATION FOR SOLUTIONS OF DBSs

To give the solutions of DBSs, one has to determine the parameter α by solving Eqs. (18) and (19). From Eq. (19), we have

$$\alpha^{\pm}(\tilde{E}) = \left(\tilde{E} \pm \sqrt{\tilde{E}^2 - \left(2J_a^K\right)^2}\right)/2J_a^K \tag{A1}$$

and $|\tilde{E}| > 2J_a^K$. Therefore, Eq. (18) can be rewritten as

$$\tilde{E} - \frac{2g^2}{\tilde{E} - \Delta - J_m^K} = 2J_a^K \alpha^{\pm}(\tilde{E}) + U. \tag{A2}$$

Because $|\alpha| < 1$, we have $\alpha = \alpha^-$ when $\tilde{E} > 0$ and $\alpha = \alpha^+$ when $\tilde{E} < 0$. Thus Eq. (A2) is equivalent to

$$\frac{-2g^2}{\tilde{E} - \Delta - J_m^K} = \pm\sqrt{\tilde{E}^2 - \left(2J_a^K\right)^2} + U. \tag{A3}$$

Introducing

$$\begin{aligned} f(\tilde{E}) &\equiv -2g^2/\left(\tilde{E} - \Delta - J_m^K\right), \\ h(\tilde{E}) &\equiv \pm\sqrt{\tilde{E}^2 - \left(2J_a^K\right)^2} + U, \end{aligned} \tag{A4}$$

the solutions of Eq. (A3) can be obtained by solving $f(\tilde{E}) = h(\tilde{E})$. Therefore, the intersections of $f(\tilde{E})$ and $h(\tilde{E})$ give the solutions of $\tilde{E}$ and then the parameter α can be given from Eq. (A1). In Fig. 6, given $g = 10$, $U = 20$, $J_a = 1$, $J_m = 0$, and $\Delta = 50$, we show the intersections of $f(\tilde{E})$ and $h(\tilde{E})$.

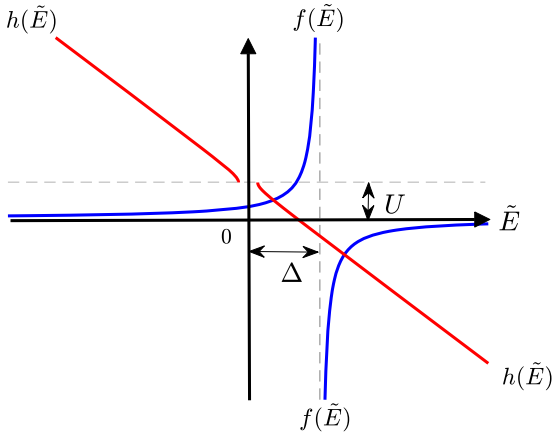

FIG. 6. Intersections of $f(\tilde{E})$ and $h(\tilde{E})$. Here, $g = 10$, $U = 20$, $J_a = 1$, $J_m = 0$, and $\Delta = 50$.

Clearly, there are always two intersections if $U = 0$, while there might be only one intersection if $U \neq 0$ for some values of Δ.

APPENDIX B: FROZEN LIMIT

In the frozen limit, $J_a = J_m = 0$, the Hamiltonian reads

$$\hat{H} = \frac{U}{2}\sum_{l=-L}^{L}\hat{n}_l^a\left(\hat{n}_l^a - 1\right) + g\sum_{l=-L}^{L}\left(\hat{a}_l^\dagger\hat{a}_l^\dagger\hat{m}_l + \text{H.c.}\right) + \sum_{l=-L}^{L}\left(\varepsilon_a\hat{n}_l^a + \varepsilon_m\hat{n}_l^m\right) \tag{B1}$$

and there are two kinds of eigenstates,

$$\begin{aligned} \left|a_{l_1,l_2}\right\rangle &= |l_1, l_2\rangle, \quad 1 \leqslant l_1 < l_2 \leqslant L_t, \\ |d_l\rangle &= A|l\rangle_m + B|l, l\rangle_a, \quad 1 \leqslant l \leqslant L_t, \end{aligned} \tag{B2}$$

where A and B are normalization coefficients. By diagonalizing the Hamiltonian (B1), one can obtain its eigenstates and eigenenergies. The eigenenergy of $|a_{l_1,l_2}\rangle$ is given as $\tilde{E}_0^0 = 0$. For $|d_l\rangle$, we have

$$\begin{aligned} \tilde{E}_1^{(0)} &= (U + \Delta - \sqrt{8g^2 + (U-\Delta)^2})/2, \\ C_1 &= A_1/B_1 = (\Delta - U - \sqrt{8g^2 + (U-\Delta)^2})/2\sqrt{2}g, \end{aligned} \tag{B3a}$$

$$\begin{aligned} \tilde{E}_2^{(0)} &= (U + \Delta + \sqrt{8g^2 + (U-\Delta)^2})/2, \\ C_2 &= A_2/B_2 = (\Delta - U + \sqrt{8g^2 + (U-\Delta)^2})/2\sqrt{2}g, \end{aligned} \tag{B3b}$$

where $A_\sigma = \pm\frac{C_\sigma}{\sqrt{1+C_\sigma^2}}$ and $B_\sigma = \pm\frac{1}{\sqrt{1+C_\sigma^2}}$ with $\sigma = \{1, 2\}$. Thus the two eigenstates read as $|d_{\sigma,i}\rangle = A_\sigma|i\rangle_m + B_\sigma|i, i\rangle_a$. These two states correspond to two isolated DBS bands.

[1] J. Kempe, Quantum random walks: An introductory overview, Contemp. Phys. **44**, 307 (2003).

[2] Y. Aharonov, L. Davidovich, and N. Zagury, Quantum random walks, Phys. Rev. A **48**, 1687 (1993).

[3] S. E. Venegas-Andraca, Quantum walks: A comprehensive review, Quantum Inf. Process. **11**, 1015 (2012).

[4] J. Du, H. Li, X. Xu, M. Shi, J. Wu, X. Zhou, and R. Han, Experimental implementation of the quantum random-walk algorithm, Phys. Rev. A **67**, 042316 (2003).

[5] B. C. Travaglione and G. J. Milburn, Implementing the quantum random walk, Phys. Rev. A **65**, 032310 (2002).

[6] A. M. Childs, Universal Computation by Quantum Walk, Phys. Rev. Lett. **102**, 180501 (2009).

[7] E. Farhi and S. Gutmann, Quantum computation and decision trees, Phys. Rev. A **58**, 915 (1998).

[8] N. Shenvi, J. Kempe, and K. Birgitta Whaley, Quantum random-walk search algorithm, Phys. Rev. A **67**, 052307 (2003).

[9] A. Ambainis, Quantum walk algorithm for element distinctness, SIAM J. Comput. **37**, 210 (2007).

[10] A. M. Childs and J. Goldstone, Spatial search by quantum walk, Phys. Rev. A **70**, 022314 (2004).

[11] B. L. Douglas and J. B. Wang, A classical approach to the graph isomorphism problem using quantum walks, J. Phys. A: Math. Theor. **41**, 075303 (2008).

[12] M. Mohseni, P. Rebentrost, S. Lloyd, and A. Aspuru-Guzik, Environment-assisted quantum walks in photosynthetic energy transfer, J. Chem. Phys. **129**, 174106 (2008).

[13] T. Kitagawa, M. A. Broome, A. Fedrizzi, M. S. Rudner, E. Berg, I. Kassal, A. Aspuru-Guzik, E. Demler, and A. G. White, Observation of topologically protected bound states in photonic quantum walks, Nat. Commun. **3**, 882 (2012).

[14] L. Xiao, X. Zhan, Z. H. Bian, K. K. Wang, X. Zhang, X. P. Wang, J. Li, K. Mochizuki, D. Kim, N. Kawakami, W. Yi, H. Obuse, B. C. Sanders, and P. Xue, Observation of topological edge states in parity–time-symmetric quantum walks, Nat. Phys. **13**, 1117 (2017).

[15] M. Karski, L. Förster, J. Choi, A. Steffen, W. Alt, D. Meschede, and A. Widera, Quantum walk in position space with single optically trapped atoms, Science **325**, 174 (2009).

[16] F. Zähringer, G. Kirchmair, R. Gerritsma, E. Solano, R. Blatt, and C. F. Roos, Realization of a Quantum Walk with One and Two Trapped Ions, Phys. Rev. Lett. **104**, 100503 (2010).

[17] H. B. Perets, Y. Lahini, F. Pozzi, M. Sorel, R. Morandotti, and Y. Silberberg, Realization of Quantum Walks with Negligible Decoherence in Waveguide Lattices, Phys. Rev. Lett. **100**, 170506 (2008).

[18] T. Fukuhara, A. Kantian, M. Endres, M. Cheneau, P. Schauß, S. Hild, D. Bellem, U. Schollwöck, T. Giamarchi, C. Gross *et al.*, Quantum dynamics of a mobile spin impurity, Nat. Phys. **9**, 235 (2013).

[19] P. L. Knight, E. Roldán, and J. E. Sipe, Quantum walk on the line as an interference phenomenon, Phys. Rev. A **68**, 020301 (2003).

[20] R. Piil and K. Mølmer, Tunneling couplings in discrete lattices, single-particle band structure, and eigenstates of interacting atom pairs, Phys. Rev. A **76**, 023607 (2007).

[21] M. Valiente and D. Petrosyan, Two-particle states in the Hubbard model, J. Phys. B **41**, 161002 (2008).

[22] J.-P. Nguenang and S. Flach, Fermionic bound states on a one-dimensional lattice, Phys. Rev. A **80**, 015601 (2009).

[23] J. Javanainen, O. Odong, and J. C. Sanders, Dimer of two bosons in a one-dimensional optical lattice, Phys. Rev. A **81**, 043609 (2010).

[24] A. Peruzzo, M. Lobino, J. Matthews, N. Matsuda, A. Politi, K. Poulios, X. Zhou, Y. Lahini, N. Ismail, K. Wörhoff *et al.*, Quantum walks of correlated photons, Science **329**, 1500 (2010).

[25] L. Sansoni, F. Sciarrino, G. Vallone, P. Mataloni, A. Crespi, R. Ramponi, and R. Osellame, Two-Particle Bosonic-Fermionic Quantum Walk via Integrated Photonics, Phys. Rev. Lett. **108**, 010502 (2012).

[26] Y. Bromberg, Y. Lahini, R. Morandotti, and Y. Silberberg, Quantum and Classical Correlations in Waveguide Lattices, Phys. Rev. Lett. **102**, 253904 (2009).

[27] A. M. Childs, D. Gosset, and Z. Webb, Universal computation by multiparticle quantum walk, Science **339**, 791 (2013).

[28] P. M. Preiss, R. Ma, M. E. Tai, A. Lukin, M. Rispoli, P. Zupancic, Y. Lahini, R. Islam, and M. Greiner, Strongly correlated quantum walks in optical lattices, Science **347**, 1229 (2015).

[29] A. Ahlbrecht, A. Alberti, D. Meschede, V. B. Scholz, A. H. Werner, and R. F. Werner, Molecular binding in interacting quantum walks, New J. Phys. **14**, 073050 (2012).

[30] Y. Lahini, M. Verbin, S. D. Huber, Y. Bromberg, R. Pugatch, and Y. Silberberg, Quantum walk of two interacting bosons, Phys. Rev. A **86**, 011603 (2012).

[31] D. Wiater, T. Sowiński, and J. Zakrzewski, Two bosonic quantum walkers in one-dimensional optical lattices, Phys. Rev. A **96**, 043629 (2017).

[32] M. Valiente and D. Petrosyan, Quantum dynamics of one and two bosonic atoms in a combined tight-binding periodic and weak parabolic potential, Europhys. Lett. **83**, 30007 (2008).

[33] X. Qin, Y. Ke, X. Guan, Z. Li, N. Andrei, and C. Lee, Statistics-dependent quantum co-walking of two particles in one-dimensional lattices with nearest-neighbor interactions, Phys. Rev. A **90**, 062301 (2014).

[34] K. Winkler, G. Thalhammer, F. Lang, R. Grimm, J. H. Denschlag, A. J. Daley, A. Kantian, H. P. Büchler, and P. Zoller, Repulsively bound atom pairs in an optical lattice, Nature (London) **441**, 853 (2006).

[35] T. Fukuhara, P. Schauß, M. Endres, S. Hild, M. Cheneau, I. Bloch, and C. Gross, Microscopic observation of magnon bound states and their dynamics, Nature (London) **502**, 76 (2013).

[36] S. Fölling, S. Trotzky, P. Cheinet, M. Feld, R. Saers, A. Widera, T. Müller, and I. Bloch, Direct observation of second-order atom tunnelling, Nature (London) **448**, 1029 (2007).

[37] N. Nygaard, R. Piil, and K. Mølmer, Feshbach molecules in a one-dimensional optical lattice, Phys. Rev. A **77**, 021601 (2008).

[38] N. Nygaard, R. Piil, and K. Mølmer, Two-channel Feshbach physics in a structured continuum, Phys. Rev. A **78**, 023617 (2008).

[39] J. C. Sanders, O. Odong, J. Javanainen, and M. Mackie, Bound states of two bosons in an optical lattice near an association resonance, Phys. Rev. A **83**, 031607 (2011).

[40] M. Grupp, R. Walser, W. P. Schleich, A. Muramatsu, and M. Weitz, Resonant Feshbach scattering of fermions in one-dimensional optical lattices, J. Phys. B **40**, 2703 (2007).

[41] D. B. M. Dickerscheid, U. Al Khawaja, D. van Oosten, and H. T. C. Stoof, Feshbach resonances in an optical lattice, Phys. Rev. A **71**, 043604 (2005).

[42] L. de Forges de Parny, V. G. Rousseau, and T. Roscilde, Feshbach-Stabilized Insulator of Bosons in Optical Lattices, Phys. Rev. Lett. **114**, 195302 (2015).

[43] C. Chin, R. Grimm, P. Julienne, and E. Tiesinga, Feshbach resonances in ultracold gases, Rev. Mod. Phys. **82**, 1225 (2010).

[44] J. Weiner, V. S. Bagnato, S. Zilio, and P. S. Julienne, Experiments and theory in cold and ultracold collisions, Rev. Mod. Phys. **71**, 1 (1999).

[45] A. Fioretti, D. Comparat, A. Crubellier, O. Dulieu, F. Masnou-Seeuws, and P. Pillet, Formation of Cold Cs_2 Molecules through Photoassociation, Phys. Rev. Lett. **80**, 4402 (1998).

[46] M Valiente and D Petrosyan, Scattering resonances and two-particle bound states of the extended Hubbard model, J. Phys. B **42**, 121001 (2009).

[47] C. Menotti, F. Minganti, and A. Recati, Momentum-dependent pseudospin dimers of coherently coupled bosons in optical lattices, Phys. Rev. A **93**, 033602 (2016).

[48] N. Syassen, D. M. Bauer, M. Lettner, D. Dietze, T. Volz, S. Dürr, and G. Rempe, Atom-Molecule Rabi Oscillations in a Mott Insulator, Phys. Rev. Lett. **99**, 033201 (2007).

[49] E. A. Donley, N. R. Claussen, S. T. Thompson, and C. E Wieman, Atom-molecule coherence in a Bose-Einstein condensate, Nature (London) **417**, 529 (2002).

[50] M. Takahashi, Half-filled Hubbard model at low temperature, J. Phys. C **10**, 1289 (1977).

[51] A. S. Solntsev, A. A. Sukhorukov, D. N. Neshev, and Y. S. Kivshar, Spontaneous Parametric Down-Conversion and Quantum Walks in Arrays of Quadratic Nonlinear Waveguides, Phys. Rev. Lett. **108**, 023601 (2012).

[52] D. A. Antonosyan, A. S. Solntsev, and A. A. Sukhorukov, Single-photon spontaneous parametric down-conversion in quadratic nonlinear waveguide arrays, Opt. Commun. **327**, 22 (2014), special issue on Nonlinear Quantum Photonics.

[53] A. S. Solntsev, F. Setzpfandt, A. S. Clark, C. W. Wu, M. J. Collins, C. Xiong, A. Schreiber, F. Katzschmann, F. Eilenberger, R. Schiek, W. Sohler, A. Mitchell, C. Silberhorn, B. J. Eggleton, T. Pertsch, A. A. Sukhorukov, D. N. Neshev, and Y. S. Kivshar, Generation of Nonclassical Biphoton States through Cascaded Quantum Walks on a Nonlinear Chip, Phys. Rev. X **4**, 031007 (2014).

[54] T. Guerreiro, A. Martin, B. Sanguinetti, J. S. Pelc, C. Langrock, M. M. Fejer, N. Gisin, H. Zbinden, N. Sangouard, and R. T. Thew, Nonlinear Interaction between Single Photons, Phys. Rev. Lett. **113**, 173601 (2014).